



**HAL**  
open science

# Enhancing Mixing During Groundwater Remediation via Engineered Injection-Extraction: The Issue of Connectivity

Oriol Bertran, D Fernàndez-garcia, Guillem Sole-mari, P Rodríguez-escales

► **To cite this version:**

Oriol Bertran, D Fernàndez-garcia, Guillem Sole-mari, P Rodríguez-escales. Enhancing Mixing During Groundwater Remediation via Engineered Injection-Extraction: The Issue of Connectivity. *Water Resources Research*, 2023, 59 (7), pp.e2023WR034934. 10.1029/2023wr034934 . insu-04158302

**HAL Id: insu-04158302**

**<https://insu.hal.science/insu-04158302>**

Submitted on 11 Jul 2023

**HAL** is a multi-disciplinary open access archive for the deposit and dissemination of scientific research documents, whether they are published or not. The documents may come from teaching and research institutions in France or abroad, or from public or private research centers.

L'archive ouverte pluridisciplinaire **HAL**, est destinée au dépôt et à la diffusion de documents scientifiques de niveau recherche, publiés ou non, émanant des établissements d'enseignement et de recherche français ou étrangers, des laboratoires publics ou privés.



Distributed under a Creative Commons Attribution 4.0 International License

# Enhancing Mixing During Groundwater Remediation via Engineered Injection-Extraction: The Issue of Connectivity

O. Bertran<sup>1,2</sup>, D. Fernàndez-Garcia<sup>1,2</sup>, G. Sole-Mari<sup>3</sup>, P. Rodríguez-Escales<sup>1,2</sup>

<sup>1</sup>Department of Civil and Environmental Engineering (DECA), Universitat Politècnica de Catalunya (UPC), Jordi Girona 1-3, 08034 Barcelona, Spain

<sup>2</sup>Associated Unit: Hydrogeology Group (UPC-CSIC)

<sup>3</sup>Géosciences Rennes, Université de Rennes, France

## Key Points:

- The spreading and dilution of a treatment solution is tested under rotating-dipole Engineered Injection-Extraction (EIE)
- EIE is similarly effective in both Multigaussian log-conductivity fields and well-connected non-Multigaussian fields
- EIE reduces the remediation outcome uncertainty associated to porous medium heterogeneity and connectivity

---

Corresponding author: Oriol Bertran, [oriol.bertran.oller@upc.edu](mailto:oriol.bertran.oller@upc.edu)

This article has been accepted for publication and undergone full peer review but has not been through the copyediting, typesetting, pagination and proofreading process, which may lead to differences between this version and the [Version of Record](#). Please cite this article as [doi: 10.1029/2023WR034934](https://doi.org/10.1029/2023WR034934).

This article is protected by copyright. All rights reserved.

## Abstract

In the context of in-situ groundwater remediation, mixing is vital for a successful outcome. A slow mixing rate between the contaminated groundwater and the injected treatment solution can severely weaken the effective degradation rate. Engineered Injection-Extraction (EIE) has been proposed as a means to accelerate dilution within the porous medium. However, existing studies on the subject have not considered the potential impact of connectivity and preferential flow-paths. Neglecting connectivity can lead to an overestimation of EIE's capabilities, since the fluid may in reality be carried mainly through a few high-permeability channels, thus hampering mixing and reaction. Due to the fact that channeling can be found in many actual sites, in this work we aim to evaluate EIE methods in both poorly-connected (represented as Multigaussian fields) and well-connected fields (represented as non-Multigaussians). The approach is to identify, for each given medium, a stirring protocol – defined by a specific combination of rotation angle and rotation rate – which maximizes mixing. To that end, metrics are proposed in order to (1) quantify both the mixing and the containment of the treatment solution within a given remediation volume, and (2) characterize the particle trajectories to explicitly evaluate if preferential paths are broken. The results obtained from these metrics are quite similar for both types of fields, proving that the enhancing of mixing by means of EIE is effective regardless of the presence of preferential flow paths. This study demonstrates that EIE via rotating dipoles diminishes the remediation outcome uncertainty induced by medium heterogeneity.

## 1 Introduction

Most *in-situ* groundwater remediation schemes are based on the injection of a treatment solution into the subsurface in order to promote reactions that remove or transform the contaminants into harmless products. For instance, the success of both bioremediation and *in-situ* chemical oxidation is based on the mixing between contaminated groundwater and nutrients or oxidant agents, which can promote the occurrence of target reactions and facilitate pollution removal. These systems can be enhanced by favoring increased mixing, that is, by promoting mass transfer between the different solutions. The physical processes that boost mass transfer in porous media are mechanical dispersion and molecular diffusion (Tartakovsky, 2010). The former spreads a solute throughout the porous medium, increasing contact surface and concentration gradients, and the latter homogenizes it leading the solute to occupy a larger volume in the porous medium. However, these processes are typically slow in natural conditions, and thus are often unable to provide sufficient mixing – and hence degradation.

Mixing in porous media has received much attention in the last few decades, largely because chemical reactions in the subsurface are often limited by mixing (Sturman et al., 1995; Cirpka et al., 1999; Cirpka, 2002; de Simoni et al., 2005; Rolle et al., 2008). In the context of groundwater remediation, some authors have proposed Engineered Injection-Extraction (EIE) as a method to promote mixing and, consequently, reactions in porous media (e.g., Zhang et al., 2009; Lester et al., 2010; Trefry et al., 2012; Piscopo et al., 2013). EIE involves a sequence of injections and extractions through wells with time-dependent flow rates, resulting in transient velocity fields which stretch and fold the solute plume (Bagtzoglou & Oates, 2007). It has been demonstrated that EIE can generate chaotic advection in porous media (Metcalfe et al., 2008; Lester et al., 2009, 2010; Trefry et al., 2012). This phenomenon, first coined in such terms by Aref (1984), is typically characterized by particle trajectories which experience exponential stretching over time, resulting in complex patterns and a virtually unpredictable evolution from the initial condition (Lester et al., 2018; Turuban et al., 2019). EIE schemes increase the active spreading and the area occupied by the injected fluid in aquifers, favoring mixing and accelerating the natural attenuation and degradation of contaminants. The benefits of this strategy has been proven for many configurations of extraction/injection wells through

68 numerical simulations (e.g., Piscopo et al., 2013; Neupauer et al., 2014; Di Dato et al.,  
69 2018; Speetjens et al., 2021), laboratory experiments (e.g., Zhang et al., 2009; Sather et  
70 al., 2023) and field applications (Cho et al., 2019). Most recently, EIE has also been demon-  
71 strated to enhance NAPL recovery in multiphase flow systems (Wang et al., 2022).

72 Several schemes can be used to create time-dependent velocity fields via EIE. Bagtzoglou  
73 and Oates (2007) and Zhang et al. (2009), used an oscillatory pumping scheme consist-  
74 ing of three randomly located wells with some realistic constraints to avoid dewatering  
75 and preserve mass. Mays and Neupauer (2012), Piscopo et al. (2013) and Neupauer et  
76 al. (2014), employed a four-well configuration operating sequentially, alternating between  
77 injection and extraction and only using one well at a time. Using a purely mathemat-  
78 ical approach, Lester et al. (2009) studied a temporally rotating 2D dipole scheme. Al-  
79 though recirculation of the treatment solution from the extraction to the injection well  
80 can exist in EIE systems, most of the previous literature has not addressed this issue.  
81 Recirculation can also enhance mixing and thus the effectiveness of the *in situ* remedi-  
82 ation system (Cirpka & Kitanidis, 2001), since it extends the residence time of the treat-  
83 ment solution within the reactive zone (Luo et al., 2007). However, frequent recircula-  
84 tion could generate bioclogging near the injection wells during bioremediation schemes  
85 (McCarty et al., 1998; Cirpka et al., 1999; MacDonald et al., 1999a, 1999b; Gandhi et  
86 al., 2002). Yet, little is known about the role of recirculation in EIE applications.

87 Mixing aside, solute transport in porous media is highly dependent on the spatial  
88 variability of hydraulic conductivity (heterogeneity) and also the presence of preferen-  
89 tial flow paths. The observations of anomalous transport and scale effects can often be  
90 associated with the omission of connectivity features (Boggs & Adams, 1992; Schulze-  
91 Makuch & Cherkauer, 1998). Connectivity in hydrogeology refers to the prevalence of  
92 higher-conductivity (K) paths that can carry and accelerate the transport of solutes from  
93 one region to another, largely bypassing the lower-conductivity areas (Knudby & Car-  
94 rera, 2005; Renard & Allard, 2013). High connectivity is thus a true hindrance in the  
95 application of a remediation scheme since it can dominate the transport of the injected  
96 solution (McGregor & Benevenuto, 2021). Yet, specific information about medium con-  
97 nectivity is usually omitted due to: (1) the lack of exhaustive geological/hydrogeological  
98 data and (2) the selection of inadequate models to characterize the heterogeneity of the  
99 porous media.

100 Regarding the latter point, the most common approach for characterizing the spa-  
101 tial variability of the log-conductivity fields is the use of two-point – also called variogram-  
102 based – geostatistics (Hashemi et al., 2014) and Multigaussian random fields, which are  
103 characterized by their mean, variance and covariance function. These multigaussian mod-  
104 els are mathematically simple and easy to treat analytically, yet they cannot reproduce  
105 high-connectivity patterns. Some non-Multigaussian models, on the other hand, are ca-  
106 pable of emulating high connectivity by arranging the high log-K values as channels (Gmez-  
107 Hernandez & Wen, 1998). Although several studies conclude that EIE can enhance mix-  
108 ing in Multigaussian heterogeneous porous media (Rodríguez-Escales et al., 2017), the  
109 applicability of EIE in real settings featuring strong preferential flow paths is still not  
110 clear.

111 Remediation efficiency depends on the degree of mixing of the treatment solution  
112 within the target treatment zone, typically defined based on the areal extent of contam-  
113 ination. In this context, transport of this solution beyond the treatment zone represents  
114 a waste of resources which should be taken into consideration. Surprisingly, dilution met-  
115 rics for permeable control volumes have not been proposed in the literature of solute trans-  
116 port in porous media, which has essentially focused on infinite domains (Kitanidis, 1994).

117 This work is aimed at studying how EIE systems based on rotating dipoles (Metcalf  
118 et al., 2008) enhance dilution in a remediation scenario and help break the preferential  
119 flow paths that often exist in highly heterogeneous aquifers. For that, we evaluate how

different EIE configurations improve (1) the dilution of an injected solution in an active remediation volume, and (2) the ability of treatment solution particles to fully explore the medium. Through a set of Monte Carlo simulations we explore different EIE configurations within both Multigaussian and well-connected non-Multigaussian log-conductivity fields.

## 2 The Engineered Injection-Extraction Method

We study an Engineered Injection-Extraction (EIE) setup based on a rotating dipole, emulating the idealized Rotated Potential Mixing (RPM) system (e.g. Metcalfe et al., 2008; Lester et al., 2009; Trefry et al., 2012). The procedure's goal is to enhance the mixing, within a circular treatment zone of radius  $R_r$ , of a treatment solution initially delivered at its center  $(x_0, y_0)$ . The treatment zone encompasses the contaminated region of the aquifer, and the determination of its size in relation to the positioning of wells is decided case-by-case attending the properties of the media and the distribution of pollutants. As a general rule, its radius ( $R_r$ ) is larger than the radius of the dipoles ( $R$ ) itself to prevent mass from immediately leaving the treatment area upon reinjection.

At  $t=0$ , the treatment solution is assumed to be uniformly distributed within a concentric circular region with radius  $r_i < R_r$ . We wish that the injected treatment solution: (1) effectively mixes with the resident groundwater; and (2) stays within the treatment zone during remediation. That is to say that we wish to transform the treatment zone into a well-mixed reactor. The treatment solution is stirred by a 2D dipole system that consists of two active wells (one injector and one extractor) separated by a distance  $2R$  that operate at the same time with a constant flow rate  $Q$ . The injection and extraction wells are symmetrically placed around the center of the domain and periodically re-oriented (emulating a larger circular array where only two wells are active at a given time). The pumped water from the extraction well is recirculated instantaneously into the injection well. Figure 1(a) shows a sketch diagram of the setup. The parameters adopted are summarized in Table 1.

During EIE operations, the dipole wells are periodically activated for a rotation period  $\tau$ , after which the active dipole position rotates counter-clockwise around the origin by an angle  $\Theta$  and operates again for a time  $\tau$ , and so on. We define the characteristic dipole-zone emptying time  $t_c$  as the time needed to renew the entire volume of water occupied within the wells zone at a constant flow rate, that is,  $t_c = \pi R^2 b \phi / Q$ , where  $\phi$  is the porosity and  $b$  is the aquifer thickness. The dimensionless time is then defined in this work as  $t^* = t/t_c$ . A range of values for the rotation angle  $\Theta$  (11 values from  $\pi/5$  to  $\pi$ ) and the rotation period  $\tau$  (25 values from  $\tau=0.05t_c$  to  $\tau=10t_c$ ) are tested, resulting in a total of 275 combinations (stirring protocols). In the following, the rotation period and the angle of rotation will be presented in normalized form, defined as  $\tau^* = \tau/t_c$  and  $\Theta^* = \Theta/\pi$ .

## 3 Flow and transport simulations

We solve flow and transport in a two-dimensional confined square aquifer of size  $L$ . The control volume and the treatment solution are located at the center of the domain,  $x_0 = L/2$  and  $y_0 = L/2$ . In all outer boundaries a no-flow condition is imposed. Regional flow is neglected for simplicity. The hydraulic conductivity is assumed locally isotropic but spatially heterogeneous. To simplify the system, we consider that dipole flows are time-dependent but piecewise steady. Consequently, groundwater flow is described by the following equation,

$$\nabla \cdot [\mathbf{K}(\mathbf{x})b\nabla h(\mathbf{x}, t)] + Q\delta(\mathbf{x} - \mathbf{x}^+(t)) - Q\delta(\mathbf{x} - \mathbf{x}^-(t)) = 0, \quad (1)$$

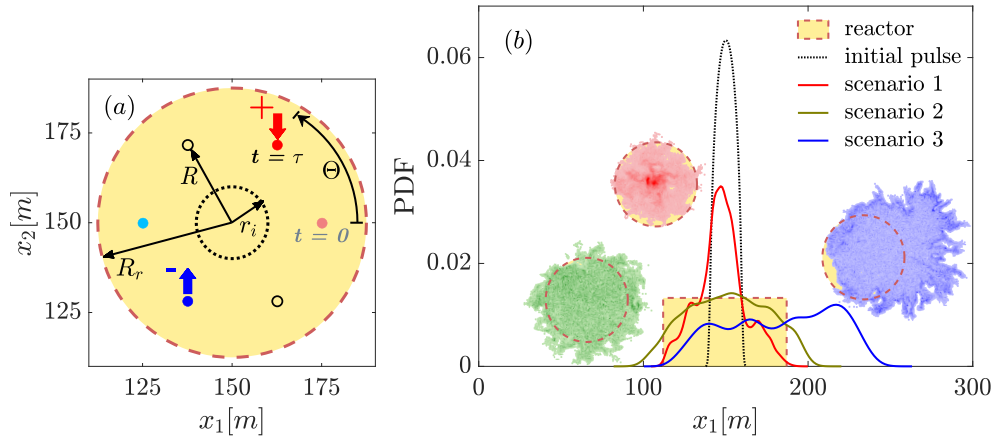


Figure 1: (a) Conceptualization of the model setup. The left figure shows 6 wells forming 3 dipoles separated by a radius  $R$ . The circular treatment area is determined by a radius  $R_r$ , and  $r_i$  delineates the area of injection. Periodically, every time lapse  $\tau$ , the active EIE dipole rotates by an angle  $\Theta$ ; (b) Three representative scenarios are shown, each one being the result of a different combination of  $\Theta$  and  $\tau$ . Two of them, the scenarios 1 and 3, display undesirable outcomes of insufficient dilution and ineffective containment, respectively. The scenario 2, in green, represents the desired outcome, featuring: (i) high dilution, and (ii) effective containment of the solute within the reactor.

Table 1: Parameters that define the conceptual EIE model

Parameters		Values
Treatment solution radius	$r_i$	10 m
Dipole radius	$R$	25 m
Reactor radius	$R_r$	37.5 m
Aquifer thickness	$b$	10 m
Aquifer length	$L$	300.25 m
Characteristic time	$t_c$	10 d
Porosity	$\phi$	0.25
Injection-Extraction rate	$Q$	491 m <sup>3</sup> /d
Amount of treatment solution particles		30000
Normalized rotation angle	$\Theta^*$	$\{\frac{1}{5}; \frac{1}{4}; \frac{1}{3}; \frac{2}{5}; \frac{1}{2}; \frac{3}{5}; \frac{2}{3}; \frac{3}{4}; \frac{4}{5}; \frac{9}{10}; 1\}$
Normalized rotation period	$\tau^*$	$\{0.05; 0.1; 0.15; 0.2; 0.3; 0.4; 0.6; 0.8; 1; 1.2; 1.4; 1.6; 1.8; 2; 2.4; 2.8; 3.2; 3.6; 4; 4.8; 5.6; 6.4; 7.2; 8; 10\}$

166 where  $\mathbf{K}(\mathbf{x})$  is the hydraulic conductivity at the  $\mathbf{x}$  location,  $b$  is the aquifer thickness (as-  
 167 sumed constant),  $h(\mathbf{x}, t)$  is the hydraulic head,  $\delta(\mathbf{x})$  is the Dirac delta function, and  $\mathbf{x}^+$   
 168 and  $\mathbf{x}^-$  are the injection and extraction positions of the rotating dipole,

$$x^\pm(t) = x_0 \pm R \cos\left(f\left(\frac{t}{\tau}\right)\Theta\right), \quad y^\pm(t) = y_0 \pm R \sin\left(f\left(\frac{t}{\tau}\right)\Theta\right), \quad (2)$$

169 where  $\Theta$  is the rotation angle,  $\tau$  is the rotation period and  $f$  is the floor function defined  
 170 as  $f(x) = \max\{n \in \mathbb{Z} | n \leq x\}$ . The transport of the treatment solution is described  
 171 by the Advection-Dispersion equation (ADE):

$$\phi \frac{\partial c}{\partial t}(\mathbf{x}, t) = -\nabla \cdot (\mathbf{q}(\mathbf{x}, t)c(\mathbf{x}, t)) + \nabla \cdot (\phi \mathbf{D}(\mathbf{x}, t) \nabla c(\mathbf{x}, t)), \quad (3)$$

where  $c(\mathbf{x}, t)$  is the solute concentration,  $\mathbf{q}(\mathbf{x}, t)$  is the Darcy velocity,  $\phi$  is the porosity  
 (assumed constant), and  $\mathbf{D}(\mathbf{x}, t)$  is the local dispersion tensor. For simplicity and since  
 mixing is typically controlled by local transverse (rather than longitudinal) dispersion,  
 we assume that  $\mathbf{D}(\mathbf{x}, t)$  is locally isotropic,

$$\mathbf{D}(\mathbf{x}, t) = \alpha \|\mathbf{v}(\mathbf{x}, t)\| \mathbf{I}_d, \quad (4)$$

172 where  $\alpha$  is the constant dispersivity,  $\|\mathbf{v}(\mathbf{x}, t)\|$  is the norm of the fluid velocity vector at  
 173 any  $\mathbf{x}$  location and time  $t$  (with  $\mathbf{v}(\mathbf{x}, t) = \mathbf{q}(\mathbf{x}, t)/\phi$ ), and  $\mathbf{I}_d$  is the identity matrix. A  
 174 value of  $\alpha = 0.25$  m is set. This yields a Péclet number (defined here as the ratio be-  
 175 tween dipole radius and dispersivity) of 1000.

176 To solve Eq. (1) we use the finite-difference code MODFLOW 2005 (Harbaugh et  
 177 al., 2017), with the Preconditioned Conjugate-Gradient method (PCG). The model do-  
 178 main is discretized into  $1201 \times 1201$  square cells of size  $\Delta = 0.25$  m. The resulting cell-  
 179 interface fluxes are then used to solve the advection-dispersion equation (ADE) by means  
 180 of the Random-Walk Particle Tracking method (RWPT). The RWPT simulations are  
 181 performed by initially distributing 30000 particles uniformly within the circular treat-  
 182 ment solution. The results have been verified to have converged for this number of par-  
 183 ticles. The RWPT method used here is based on the approach of LaBolle et al. (2000),  
 184 which is suitable for simulating transport through porous media in systems with abrupt  
 185 changes in dispersion. The formal derivation and details of this RWPT method are not  
 186 presented here; the interested reader may refer to the source itself or other works such  
 187 as Delay et al. (2005), Salamon et al. (2006) or Sole-Mari et al. (2021).

188 The scattered data points of the particle positions are then reconstructed into con-  
 189 centrations using an open-source MATLAB code developed by Sole-Mari et al. (2019).  
 190 With this approach, concentrations are efficiently reconstructed by combining histogram  
 191 methods with locally adaptive Kernel Density Estimation methods. This makes the es-  
 192 timation of concentration efficient, robust and less restrictive on the number of particles.

## 193 4 Stochastic approach

194 Monte Carlo simulations are performed to represent multiple equiprobable reali-  
 195 ties of the natural logarithm of the hydraulic conductivity field  $Y(\mathbf{x}) = \ln K(\mathbf{x})$ , which  
 196 is described as a random function of space. We generate 50 Multigaussian and 50 non-  
 197 Multigaussian random fields (Fig. 2). The difference between Multigaussian (MG) and  
 198 the particular type of non-Multigaussian (nMG) fields is that the former have the ex-  
 199 treme values of  $Y(\mathbf{x})$  isolated from the rest and the latter have the higher values con-  
 200 nected. Both MG and nMG fields share similar two-point statistical properties: (1) iden-  
 201 tical log-normal hydraulic conductivity distribution and (2) near-identical isotropic spa-  
 202 tial covariance function.

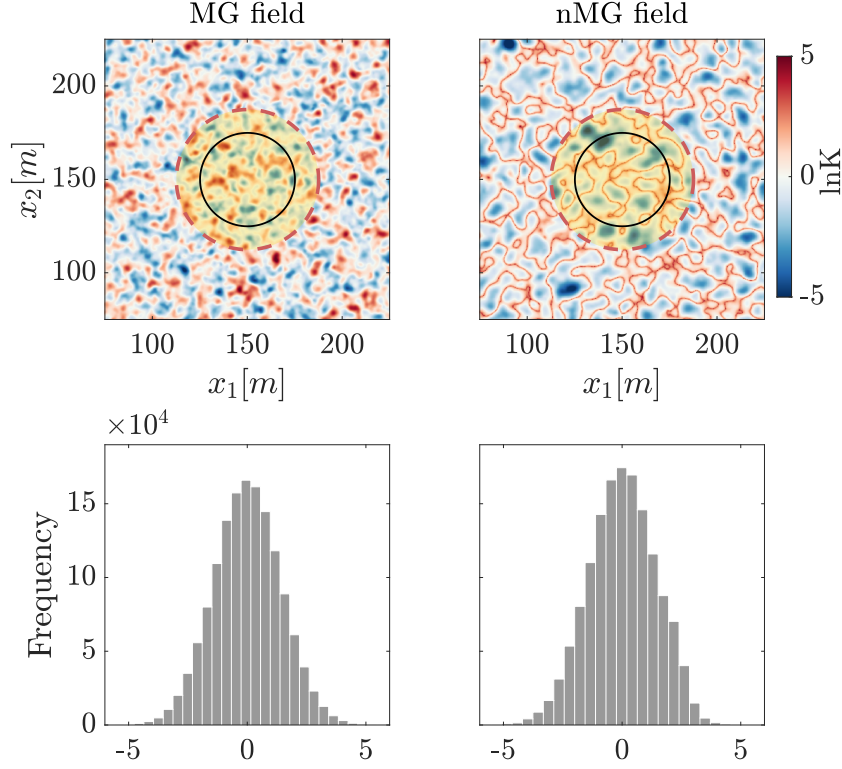


Figure 2: Central region of two selected Multigaussian and connected non-Multigaussian fields used in the simulations. the wells zone is represented with a solid line, and the treatment zone with a dashed line. Below, the corresponding histograms of  $Y = \ln K$ .

MG fields are generated using the SGeMS software (Remy, 2005) via the sequential Gaussian simulation subroutine SGSIM with zero mean, variance  $\sigma_Y^2 = 2$ , and an isotropic Gaussian covariance function model with a range of  $a=5$  meters, which is 10% of the distance between injection and extraction wells in a dipole. This relatively low range results in a somewhat poor hydraulic connection between the injection and extraction wells. nMG fields, on the other hand, are specifically generated to display high connectivity of high values that favor the formation of preferential flow paths. We use the method developed by Zinn and Harvey (2003), which transforms any MG field into a nMG field by (1) normal scoring the MG field; (2) taking the absolute value; and (3) transforming the distribution of absolute values into a log-normal distribution with zero mean and  $\sigma_Y^2$  variance:

$$Y' = -\sigma_Y \sqrt{2} \operatorname{erf}^{-1} \left( 2 \operatorname{erf} \left( \frac{Y}{\sqrt{2}} \right) - 1 \right), \quad (5)$$

where  $Y'$  are the transformed values and  $Y$  are the absolute values obtained in the previous step. This rearrangement reduces the integral scale of the random field by a factor of 1.86 (yellow line in Fig. 3). This is addressed by resizing the field by a factor of 1.86 and then cropping it also by a factor of 1.86 in order to keep the same domain size for both random field types.

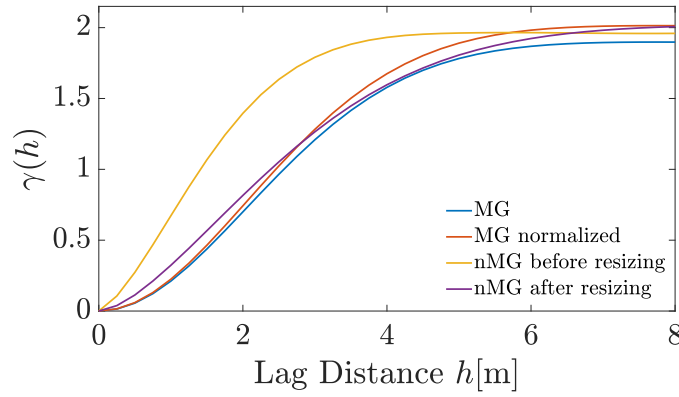


Figure 3: The different spatial semivariograms obtained during the transformation procedure from one selected MG to the nMG field

## 5 Performance metrics

### 5.1 Volume-control reactor efficiency

We aim to quantify the degree of mixing within the treatment zone, a fixed control volume  $V$  defined previously based on remediation targets and the areal extent of contamination ( $R_r$  in Figure 1(a)). In order to reduce remediation costs and risks, the treatment solution should only spread and mix within the contaminated area. In this context, it is convenient to have a metric that quantifies the degree of mixing within the remediation target volume. Kitanidis (1994) defines the reactor ratio  $M$  as the ratio of the actual dilution index  $E$  of a solute plume in a volume  $V$  to its maximum theoretical value  $E_{max}$ ,

$$M = \frac{E}{E_{max}}. \quad (6)$$

The dilution index is defined as

$$E(t) = \exp \left[ - \int_V p(\mathbf{x}, t) \ln(p(\mathbf{x}, t)) dV \right], \quad (7)$$

where  $p(\mathbf{x}, t)$  is the probability density for a mass particle to be located on  $\mathbf{x}$  at time  $t$ ,

$$p(\mathbf{x}, t) = \frac{\phi c(\mathbf{x}, t)}{\int_V \phi c(\mathbf{x}, t) d\mathbf{x}}. \quad (8)$$

The dilution index  $E$  is a well-established metric of dilution that quantifies the volume occupied by the solute plume in  $V$  (Kitanidis, 1994). Note for instance that when the solute is uniformly distributed in the aquifer over a volume  $W$  ( $W < V$ ), assuming constant porosity,  $p$  approaches  $1/W$  and  $E$  tends to  $W$ , which is the volume occupied by the solute. The reactor ratio  $M$  can thus be interpreted as the fraction of the volume  $V$  occupied by the solute plume, i.e., in this example we have that  $M = W/V$ . Thus,  $M$  is a dimensionless number that ranges between 0 and 1. The larger the value of  $M$ , the closer the system is to well-mixed conditions (complete mixing). Also note that, in our case, maximum dilution in  $V$  is achieved when

$$E = E_{max} = V = \pi R_r^2 b \phi. \quad (9)$$

240 Kitanidis (1994) defines the reactor ratio  $M$  for two specific cases only: a bounded  
 241 and an unbounded system. Neither of these cases accurately describes our system. The  
 242 former would imply the assumption of a closed system where the injected solution can-  
 243 not leave the control volume  $V$ . The latter describes the state of dilution of the plume  
 244 as it is transported within an infinite aquifer. In our case the target volume is not iso-  
 245 lated with impermeable boundaries nor is it infinite, but is a finite permeable volume  
 246 defined by remediation targets. Depending on the pumping and injection sequence used,  
 247 it is possible for a portion of the injected treatment solution to escape from the control  
 248 volume  $V$ , and that portion should not count towards the well-mixed volume metric, since  
 249 our goal is to maximize mixing within  $V$ . Hence we define the volume-control reactor  
 250 efficiency as

$$\varepsilon_V = \omega M. \quad (10)$$

251 Here,  $\omega$  is the mass fraction of the injected treatment solution that remains in  $V$   
 252 at all times, i.e.,  $\omega = m_{in}/m_{tot}$ , where  $m_{in}$  is the mass of injected solution remaining  
 253 inside of  $V$ , and  $m_{tot}$  is the total injected mass.  $\varepsilon_V$  can also be seen as a measure of the  
 254 probability that the injected treatment solution is completely diluted in the control vol-  
 255 ume  $V$ . It is therefore a dimensionless number that ranges between 0 and 1. A value close  
 256 to 0 indicates that mixing is not complete inside of  $V$  and/or is taking place outside, and  
 257 a value close to 1 indicates that the total injected solution has perfectly mixed within  
 258 the control volume  $V$  (see Scenario 2 in Fig. 1(b)).

## 259 5.2 Lagrangian semivariogram

260 An important objective of this work is to determine whether EIE can partially over-  
 261 come the detrimental effect of preferential channels on solute mixing. In this context,  
 262 the dilution index might not be sufficient in order to completely describe the interaction  
 263 between solute particles and the porous medium, since it does not provide any informa-  
 264 tion about individual particle trajectories but rather a snapshot of their global positions.  
 265 Hence we also examine the Lagrangian semivariogram of  $Y(\mathbf{X}_p(t))$  values visited by par-  
 266 ticles along their paths,

$$\gamma(t') = \frac{1}{2} E \left[ \left( Y(\mathbf{X}_p(t+t')) - Y(\mathbf{X}_p(t)) \right)^2 \right], \quad (11)$$

267 where  $E$  is the expected value operator, and  $t'$  is the time lag between any two parti-  
 268 cle positions. This Lagrangian semivariogram measures the average degree of dissimi-  
 269 larity (in terms of log-conductivity) between the zones visited by the particles.

270 Note, however, that during EIE the recirculation of particles from extraction to in-  
 271 jection well can produce artificial jumps that do not reflect the temporal persistence of  
 272 particles moving through similar conductivity zones. To avoid this, the Lagrangian semi-  
 273 variogram is computed by segmenting the particle trajectories into different paths. A par-  
 274 ticle path is defined as the concatenation of positions visited by a particle without be-  
 275 ing recirculated. Figure 4 illustrates this with an example of the  $Y$  values sampled by  
 276 one particle and its corresponding displacement. For each realization and stirring pro-  
 277 tocol, the sample semivariogram is calculated as

$$\gamma(t') \approx \frac{1}{2N(t')} \sum_{\substack{(i,j)|t'=|t_j-t_i|, \\ (i,j) \in path}} (Y_{t_i} - Y_{t_j})^2, \quad (12)$$

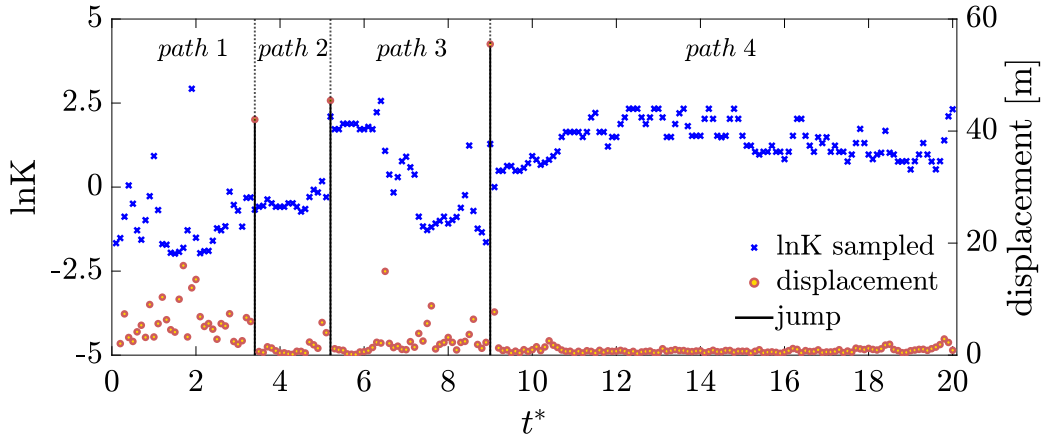


Figure 4: Values of  $\ln K$  sampled by a selected particle, and its discrete displacements during the simulation, versus cumulative dimensionless time  $t^* = t/t_c$ . Whenever a jump from the extraction to the injection well occurs, a new path is generated.

where  $Y_{t_i}$  is the  $Y$  value at the  $\mathbf{X}_p(t_i)$  position, and  $N(t')$  is the number of pairs  $(Y_{t_i}, Y_{t_j})$  such that  $t' = |t_j - t_i|$ , and  $\mathbf{X}_p(t_i)$  and  $\mathbf{X}_p(t_j)$  belong to the same path and particle trajectory.

In contrast to the dilution index, which is based on a snapshot at a given time, the Lagrangian semivariogram is an integrated metric which encapsulates the movement of particles during the entire simulation, giving valuable information about the hydrogeological response to connectivity.

The sample Lagrangian semivariogram of  $Y$  approaches a stable plateau at increasing time lags (shown later on in section 6), suggesting that, over the temporal and spatial scales of this problem, we deal with a stationary regionalized variable. Based on this, we characterize the Lagrangian semivariogram of  $Y$  by its sill ( $\sigma^2$ ) and integral scale ( $I_t$ ). The sill is estimated by the asymptote of the semivariogram and represents the range of  $Y$  values sampled by the particles. When the most frequented locations within paths have similar  $Y$  values, we have that  $\sigma^2 \ll \sigma_Y^2$ . This can occur for instance when particles concentrate their movement through preferential channels. When, on the contrary, the random field is fully sampled (complete mixing), we have that  $\sigma^2 \approx \sigma_Y^2$ . The integral time scale  $I_t$  quantifies the temporal persistence of  $Y$  values along particle paths. The greater its value, the longer the particles tend to remain in the same conductivity zone during the simulation. The integral time-scale is defined as

$$I_t = \frac{1}{\sigma^2} \int_0^\infty C(t') dt', \quad (13)$$

where  $C(t')$  is the Lagrangian covariance function of  $Y(\mathbf{X}_p(t))$ . Since, for a stationary random process,  $C(t') = \sigma^2 - \gamma(t')$ , the integral time scale can be calculated from the sample Lagrangian semivariogram by numerically solving the following limit,

$$I_t \approx \lim_{t_f \rightarrow \infty} \left[ t_f - \frac{1}{\sigma^2} \int_0^{t_f} \gamma(t') dt' \right]. \quad (14)$$

In practice, this limit is attained for  $t_f$  larger than the time lag at which the correlation vanishes.

299 During EIE, we wish to maximize the sill  $\sigma^2$  (particles' proneness to move through  
 300 different zones) and reduce the integral time scale  $I_t$  (typical residence time within zones  
 301 of similar conductivity). To quantify this in a synthesized manner, we define the follow-  
 302 ing dimensionless metric of domain sampling effectiveness,

$$\Omega = \left( \frac{\sigma^2}{\sigma_Y^2} \right) \left( \frac{t_c I_Y}{R I_t} \right), \quad (15)$$

303 where  $I_Y$  is the integral scale of the porous medium,  $I_Y = a\sqrt{\pi}/6$ , and  $a$  is the spa-  
 304 tial range of  $Y(\mathbf{x})$ .

305 In order to characterize treatment solution recirculation during EIE, We also mea-  
 306 sure the frequency of recirculation, defined as the average number of instances per unit  
 307 of time that particles recirculate through wells during operation.

## 308 6 Results and discussion

### 309 6.1 Reactor efficiency

310 We start the analysis of the results by describing the temporal evolution of the volume-  
 311 control reactor efficiency  $\varepsilon_V$  during EIE. Figure 5 shows the ensemble average of  $\varepsilon_V$  over  
 312 all realizations of (a) MG and (b) nMG random fields as a function of time for all stir-  
 313 ring protocols (combinations of  $\Theta^*$  and  $\tau^*$ ). Results show the existence of a set of opti-  
 314 mal EIE pumping sequences which achieve the highest  $\varepsilon_V$  values with a nearly stable  
 315 plateau after a few characteristic times. These optimal protocols are highlighted with  
 316 dotted lines. On the other hand,  $\varepsilon_V$  exhibits a weak or slow response, sometimes followed  
 317 by a late-time decline when a sub-optimal protocol is used.

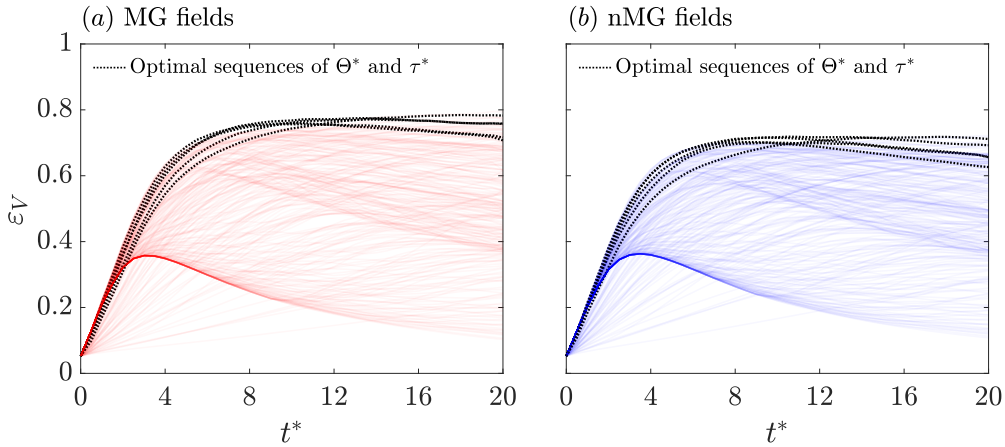


Figure 5: Temporal evolution of the volume-control reactor efficiency  $\varepsilon_V$  for every combination of  $\Theta^*$  and  $\tau^*$ , within (a) MG fields, and (b) nMG fields. Optimal stirring protocols are highlighted with dotted lines.

318 A similar temporal evolution of  $\varepsilon_V$  is observed in both MG and nMG random fields,  
 319 which are found to share the same optimal sequences of  $\Theta^*$  and  $\tau^*$ . However, nMG fields  
 320 exhibit relatively smaller optimal reactor efficiencies ( $\varepsilon_V$  decreases by about 10%). This

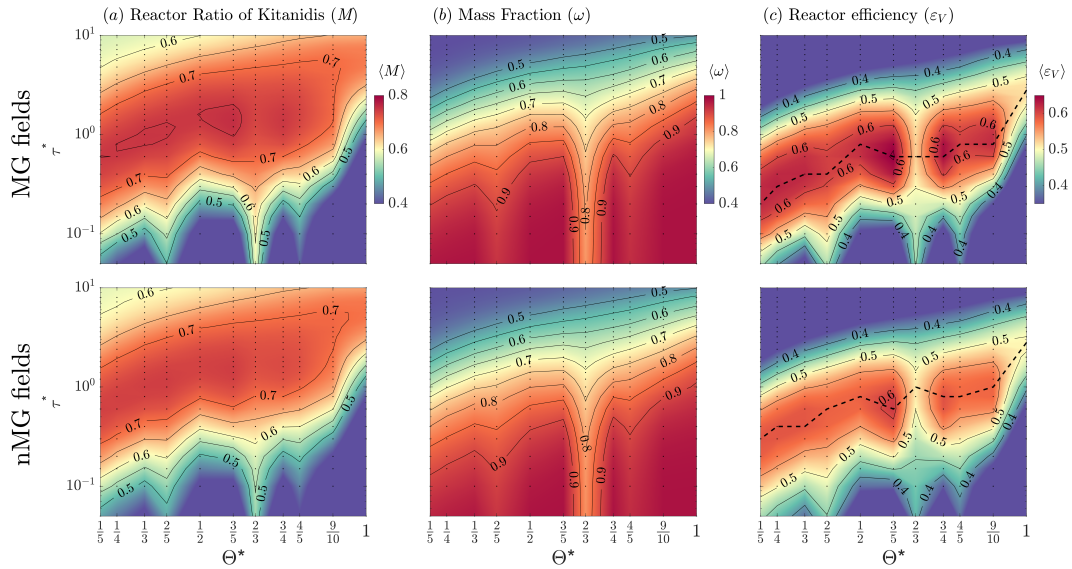


Figure 6: Ensemble average of the temporal mean over  $t^* \in [0, 20]$  of (a) the Reactor Ratio of Kitanidis  $M$ , (b) the mass fraction inside the treatment zone  $\omega$ , and (c) the volume-control reactor efficiency  $\varepsilon_V = \omega M$  as a function of  $\Theta^*$  and  $\tau^*$ , for MG and nMG fields. The dashed line in the Reactor Efficiency figures follows the maximum values of dilution found for each  $\Theta^*$ .

321 difference in efficiency between MG and nMG fields indicates that even though EIE can  
 322 significantly enhance mixing, preferential flow-paths do exert some negative impact on  
 323 its effectiveness in nMG fields. Figure 6, displays maps of the ensemble average of (a)  
 324  $M$ , (b)  $\omega$  and (c)  $\varepsilon_V = \omega M$ , averaged over  $t^* \in [0, 20]$ , as a function of  $\Theta^*$  and  $\tau^*$ , in  
 325 both MG and nMG fields. These results indicate that the connectivity of nMG fields cause  
 326 reduced dilution ( $M$ ), as well as a slightly lower ability to contain the treatment solu-  
 327 tion ( $\omega$ ) within the designated area. For a given value of  $\Theta^*$ , an exceedingly slow rota-  
 328 tion period,  $\tau^* \ll 1$ , will not stir the injected solution properly and, as a consequence,  
 329 much of the solution will stay near the injection location and will not mix substantially.  
 330 On the other hand, if the rotation period is too high,  $\tau^* \gg 1$ , a large amount of the  
 331 solution will leave the treatment zone. This is illustrated in Figure 7, where the partic-  
 332 le positions at time  $t^* = 8$  are shown for  $\tau^* \in [0.1, 1, 10]$ , and two values of  $\Theta^*$ . We  
 333 finally note from Figure 6 that, generally, the higher the rotation angle, the higher the  
 334 corresponding optimal rotation period. Actually, for  $\Theta^* < 3/5$  the optimal rotation peri-  
 335 od can be estimated as  $\tau^* \approx 2\Theta^*$ . A singular behavior occurs at  $\Theta^* = 2/3$ , where  
 336 the volume-control reactor efficiency is rather low and quite insensitive to the rotation  
 337 period. The explanation for this singular behavior is not trivial, but it is related to the  
 338 Hamiltonian of the flow field for  $\tau \rightarrow 0$  and the associated mode locking, as shown by  
 339 Lester et al. (2010).

340 Figure 8 displays the coefficient of variation (CV) of  $\varepsilon_V$ , as a function of  $\Theta^*$  and  
 341  $\tau^*$ , for MG and nMG fields. Results show that the region of maximum reactor efficiency  
 342 is also that of minimum uncertainty (CV). Hence, the EIE system proposed here to en-  
 343 hance mixing-driven reactions in predefined treatment areas not only enhances mixing,  
 344 but is also capable of reducing its uncertainty, which makes the system more reliable and  
 345 less dependent on heterogeneity. From a practical perspective, this means that EIE can  
 346 enhance remediation efficiency and reduce the risk of not reaching target remediation  
 347 goals at the same time.

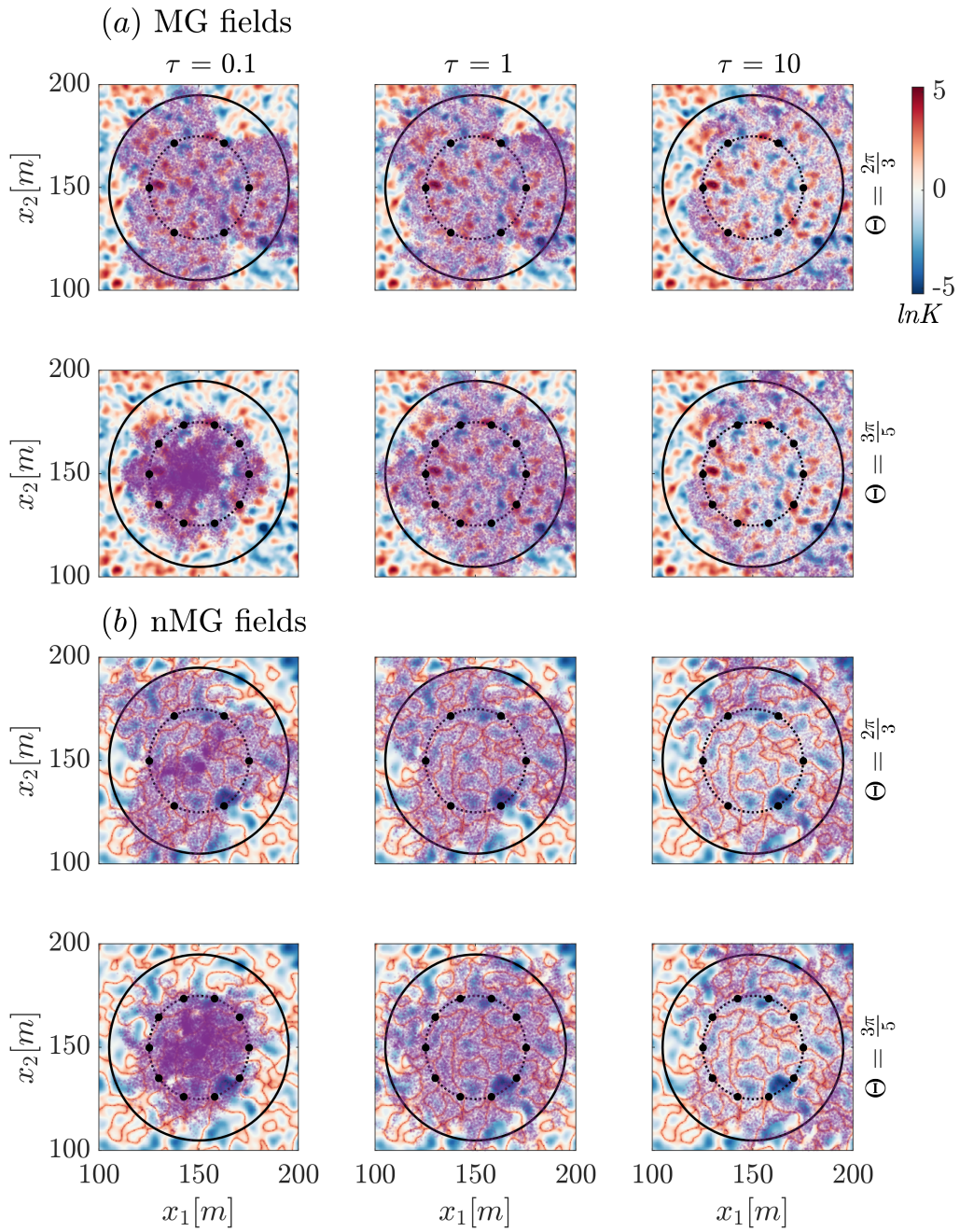


Figure 7: Particle positions at time  $t^* = 8$  with  $\tau^* \in [0.1, 1, 10]$ , for 2 configurations of  $\Theta^*$  ( $\frac{3\pi}{5}$  and  $\frac{2\pi}{3}$ ), in a representative Multigaussian field (upper two) and non-Multigaussian field (lower two). The dotted line encircles the wells area and the continuous line delimits the treatment zone.

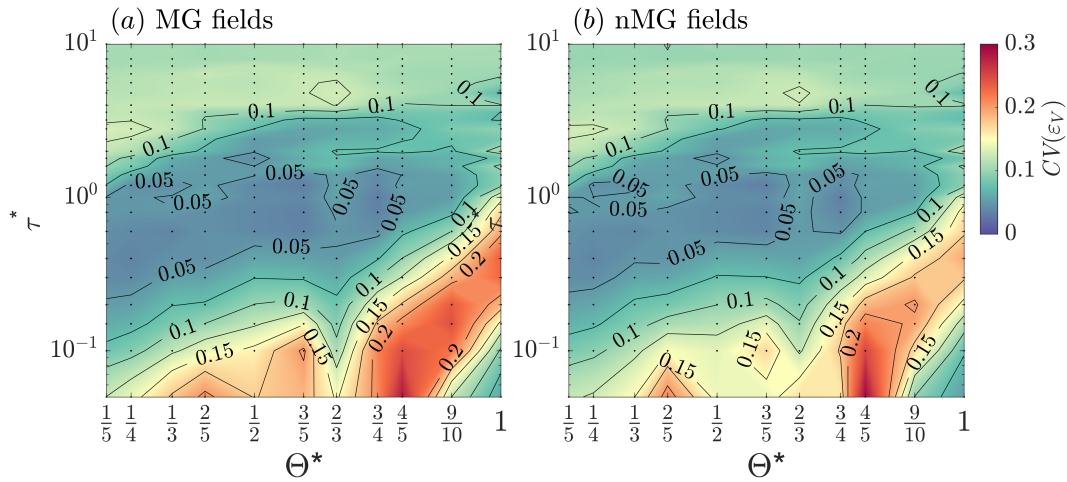


Figure 8: Coefficient of variation (CV) of  $\varepsilon_V$  as a function of  $\Theta^*$  and  $\tau^*$  for MG and nMG fields.

Similar results were obtained by Wang et al. (2022) for multiphase flow systems, where the authors demonstrated that EIE can not only enhance the removal of non-aqueous phase liquids (NAPLs) but also reduce its uncertainty. Yet, important differences exist between NAPL removal and contaminant transport. NAPL removal efficiency should first undergo an early stage with detrimental effects in order to enhance removal in the long-term. Here, we found that the optimal stirring protocols are capable of enhancing the volume-control reactor efficiency at all times.

## 6.2 Breaking the preferential flow paths

Preferential flow paths could have a detrimental effect on in-situ treatment technologies during remediation, because the injected treatment solution might concentrate in high-permeability regions, leaving a large portion of the system without treatment. We wish to understand whether the enhancement of mixing produced by the EIE system deactivates this channeling effect. For this, we examine the Lagrangian semivariogram of the  $Y$  values sampled along particle paths. While the sill ( $\sigma^2$ ) of the semivariogram quantifies the variability of  $Y$  along particle paths, the integral time-scale ( $I_t$ ) indicates how quickly these  $Y$  values are visited. We assume that if particles tend to visit a large variety of  $Y$  values in a short time, they can easily escape from preferential flow paths.

Figure 9 shows the ensemble average of the Lagrangian semivariogram over all realizations of MG (red lines) and nMG fields (blue lines), for all rotation periods and 4 representative rotation angles  $\Theta^*$ . In equivalent scenarios, MG fields always exhibit higher semivariogram values, indicating more effective spatial sampling than in nMG fields.

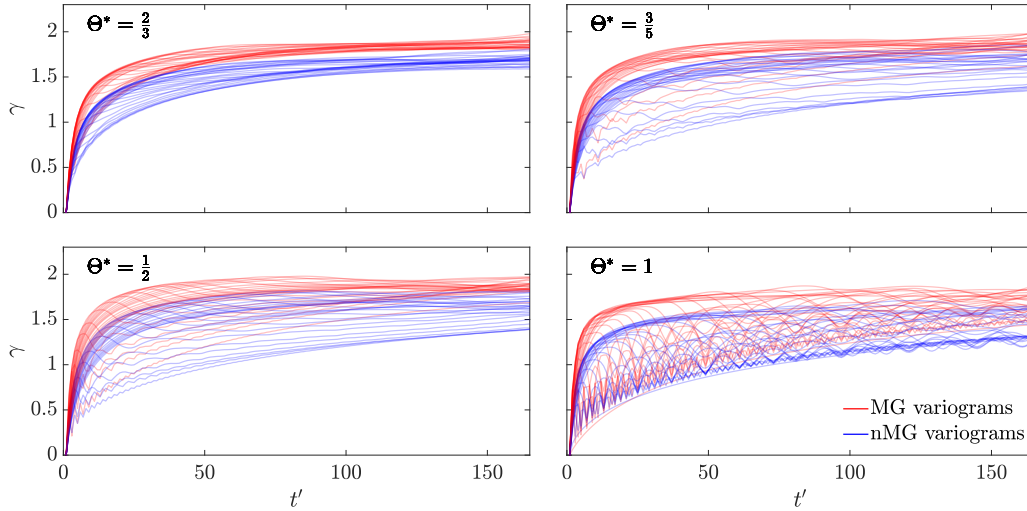


Figure 9: Ensemble average of Lagrangian semivariograms for all rotation periods  $\tau^*$  and four chosen rotation angles  $\Theta^*$ :  $\Theta^* = \frac{2}{3}$ ;  $\Theta^* = \frac{3}{5}$ ;  $\Theta^* = \frac{1}{2}$ ; and  $\Theta^* = 1$

370 The sill ( $\sigma^2$ ) and the integral time-scale ( $I_t$ ) of the Lagrangian semivariogram of  
 371  $Y$ , together with the sampling effectiveness ( $\Omega \propto \sigma^2 I_t^{-1}$ ), are depicted in Fig. 10 as a  
 372 function of  $\Theta^*$  and  $\tau^*$ . For comparison purposes, this Figure also overlaps the contour  
 373 line of  $\varepsilon_V = 0.55$ . This region of optimal dilution displays considerable overlap with  
 374 that of reduced integral time-scale ( $I_t$ ), both for MG and nMG fields. Note that a low  
 375 value of  $I_t$  suggests high propensity of zone change by particles. Hence, this result un-  
 376 derpins the notion, established in section 6.1, that the optimal protocols are capable of  
 377 partially overcoming the detrimental effect of preferential flow paths. However, nMG fields  
 378 do exhibit a noticeably lower sill ( $\sigma^2$ ) within this optimal dilution region, which is a per-  
 379 sistent consequence of their higher connectivity, and which explains the slightly lower  
 380 values of  $\varepsilon_V$  displayed by nMG fields with respect to their MG counterparts (see section  
 381 6.1 above).

382 The stirring protocols leading to maximum volume-control reactor efficiency and  
 383 sampling effectiveness are somewhat different. Sampling effectiveness requires slightly  
 384 higher rotation periods. Nevertheless, there is a region of overlap between high reactor  
 385 dilution and high Lagrangian sampling effectiveness. Note that the latter does not mea-  
 386 sure whether the particles stay within the remediation zone.

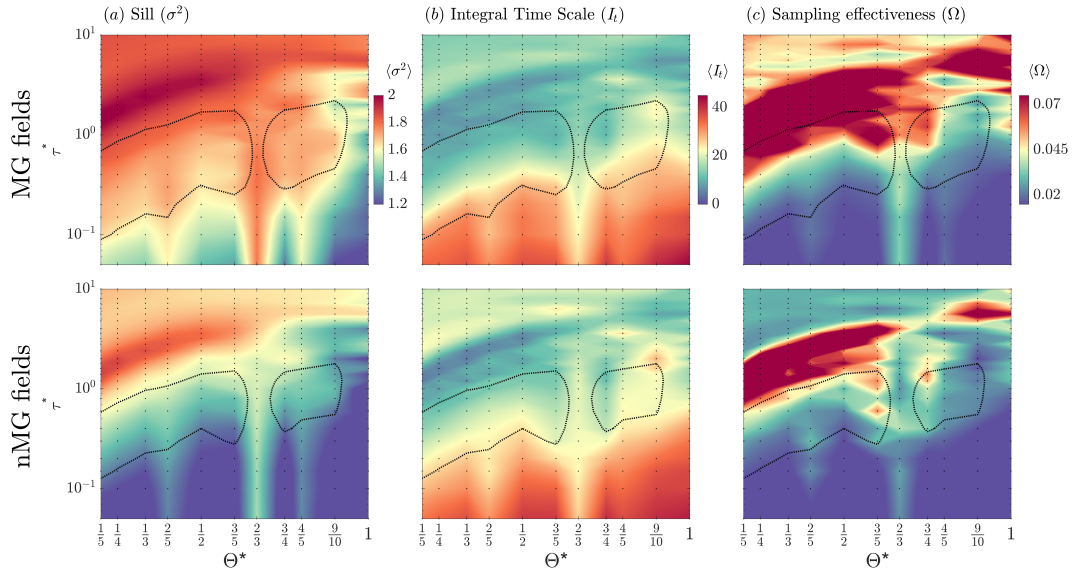


Figure 10: Zonation maps of the parameters that summarize the information given by the Lagrangian semivariograms: (a) the sill  $\sigma^2$ , (b) the integral time scale  $I_t$  and (c) the sampling effectiveness  $\Omega \propto \sigma^2 I_t^{-1}$ , as a function of  $\Theta^*$  and  $\tau^*$ , overlapped by the contour of Fig. 6(c), corresponding to  $\varepsilon_V \geq 0.55$ , considered as the optimal dilution zone.

### 6.3 On recirculation

In this section we examine the role of treatment solution recirculation between extraction and injection wells during the application of EIE. Figure 11 shows the ensemble average of the frequency of recirculation over all realizations of MG and nMG fields as a function of  $\Theta^*$  and  $\tau^*$  after all simulation time  $t^* = 20$ .

Results show that, while recirculation does clearly contribute to mixing, the overlap with the high-dilution region  $\varepsilon_V \geq 0.55$  (delimited by dotted lines) is only partial. The higher  $\tau^*$  values within this optimized region exhibit only moderate frequency of recirculation. These are the same optimal stirring protocols that display high Lagrangian sampling efficiency (which is not affected by recirculation events, see sections 5.2 and 6.2). This suggests that each of these two mechanisms – (1) heterogeneity sampling by moving through the medium, and (2) recirculation-induced mixing – contributes, separately, to the overall picture of dilution. In cases where a high recirculation rate should preferably be avoided (such as when dealing with clogging risks), this upper region of high  $\tau^*$  might be the adequate choice since it can provide high mixing efficiency with relatively low recirculation frequency. On the other hand, the singular case of  $\Theta^* = 2/3$ , which has the potentially advantageous feature of low sensitivity of  $\varepsilon_V$  to  $\tau^*$ , also displays a low frequency of recirculation. Hence, this configuration could be beneficial for the aforementioned type of field applications where clogging is a potential concern, although dilution efficiency will not be as high.

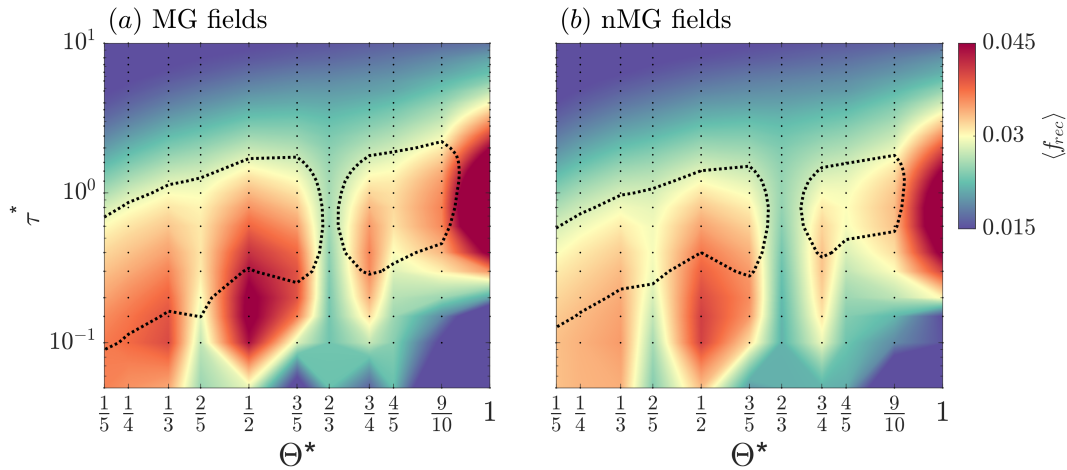


Figure 11: Ensemble average of the frequency of recirculation over  $t^* \in [0, 20]$  over all realizations of MG and nMG fields as a function of  $\Theta^*$  and  $\tau^*$ . For comparison purposes, the contour of Fig. 6(c) corresponding to the values of  $\varepsilon_V \geq 0.55$  is overlapped.

## 7 Summary and conclusions

This work assesses the use of Engineered Injection-Extraction (EIE) for enhancing the mixing between an injected treatment solution and the contaminants emplaced in a specific remediation treatment zone. Chaotic advection is generated through periodically activating well dipoles separated by a rotation angle  $\Theta$  for a period  $\tau$ . To evaluate the method, flow and transport simulations are performed for multiple realizations of randomly heterogeneous log-conductivity fields specifically designed to compare the performance of the method in MultiGaussian (MG) and high-connectivity non-MultiGaussian (nMG) fields. These nMG fields display well-connected high permeability structures that concentrate the flow in preferential paths and complicate remediation efforts.

To evaluate the performance of EIE, we propose the use of a new volume-control reactor efficiency metric  $\varepsilon_V$  which aims at maximizing both the mixing of the injected treatment solution and its containment within a designated remediation zone. In addition, Lagrangian semivariograms of  $Y$  along particle trajectories are used to explicitly evaluate whether preferential flow paths are broken during EIE. The main findings are listed below:

1. Optimal EIE stirring protocols ( $\Theta$ ,  $\tau$ ) exist which maximize the volume-control reactor efficiency within the treatment zone. These optimal stirring protocols are independent of the type of random field and its connectivity structure. For small rotation angles,  $\Theta < 3\pi/5$ , the optimal rotation period can be approximately estimated as  $\tau = 2t_c\Theta/\pi$ . From a practical point of view, there are no clear benefits in using a large number of dipoles, since the gain in volume-control reactor efficiency is not relevant compared to the increment in the number of wells and complexity of the EIE system; 2 or 3 dipoles with  $\Theta = \pi/2$  and  $\Theta = \pi/3$  seem sufficient to reach a high reactor efficiency in practical applications. An EIE system with  $\Theta = 2\pi/3$  achieves a slightly lower reactor efficiency than these optimal stirring protocols but it is less dependent on the rotation period. This can be an adequate choice in cases where the rotation period is not meant to be optimized. This singular case ( $\Theta = 2\pi/3$ ) can also be advantageous when dealing with clogging risks, since it features a low recirculation rate of the treatment solution.

- 437 2. The optimization of the stirring protocol is important for designing an adequate  
 438 EIE operation. With optimal stirring protocols, the volume-control reactor effi-  
 439 ciency increases monotonically to a maximum value after approximately 8 char-  
 440 acteristic times,  $t = 8Q/\pi R^2 b \phi$ , where  $Q$  is the pumping rate,  $R$  is the distance  
 441 between injection and extraction wells,  $b$  is the aquifer thickness, and  $\phi$  the poros-  
 442 ity. For  $\Theta < 3\pi/5$ , that is to say that EIE approaches maximum strength after  
 443 2 rotations. Suboptimal stirring protocols exhibit a weak response and/or a late-  
 444 time decline of the reactor efficiency. When  $\tau$  is too small ( $\tau \ll t_c$ ), the injected  
 445 treatment solution is trapped near the injection location, and when  $\tau$  is too high  
 446 ( $\tau \gg t_c$ ), a large amount of the injected solution is lost outside the treatment  
 447 zone.
- 448 3. Heterogeneity typically complicates remediation efforts and makes field applica-  
 449 tions highly uncertain. Optimized EIE not only enhances the mixing between the  
 450 injected treatment solution and the contaminants, but also reduces its uncertainty,  
 451 making the remediation outcome more reliable and less dependent on heterogene-  
 452 ity. This means that EIE can improve remediation effectiveness and at the same  
 453 time reduce the risk of not reaching remediation targets.
- 454 4. The presence of preferential channels in nMG fields can reduce the optimal reac-  
 455 tor efficiency of the EIE system. In our case, when  $\sigma^2=2$ , we obtain a factor of  
 456 1.14 compared to MG fields. Optimal EIE protocols can generate reduced tem-  
 457 poral correlations of visited aquifer zones along particle paths, both for MG and  
 458 nMG fields. The results lead us to conclude that EIE helps to reduce the impact  
 459 of preferential flow channels on remediation but cannot completely eliminate the  
 460 tendency of contaminants to enter into preferential channels.
- 461 5. Maximum (Eulerian) volume-control reactor efficiency and maximum (Lagrangian)  
 462 sampling effectiveness involve different stirring protocols. Sampling effectiveness  
 463 requires slightly larger rotation periods to force the particles to escape from pref-  
 464 erential channels. This effect is minor and, when wisely chosen, optimal stirring  
 465 protocols (i.e., with high volume-control reactor efficiency) also exhibit large sam-  
 466 pling effectiveness.

## 467 Acknowledgments

468 This work was financially supported by GRADIENT (PID2021-127911350-OB-100),  
 469 the Catalan Research Project RESTORA (ACA210/18/00040), and the European re-  
 470 search project MixUP (HORIZON-MSCA-2021-PF-01-101068306). Additional funding  
 471 was obtained from the Generalitat de Catalunya (2017 SGR1485). The authors thank-  
 472 fully acknowledge the computer resources at TITANI and the technical support provided  
 473 by the CaminsTECH. The output data used to elaborate the figures in section 6 is avail-  
 474 able on Zenodo (<https://doi.org/10.5281/zenodo.7753809>).

## 475 References

- 476 Aref, H. (1984). Stirring by chaotic advection. *Journal of fluid mechanics*, *143*, 1–  
 477 21.
- 478 Bagtzoglou, A. C., & Oates, P. M. (2007). Chaotic advection and enhanced ground-  
 479 water remediation. *J. Mat. Civil Eng.*, *19*, 75–83.
- 480 Boggs, J. M., & Adams, E. E. (1992). Field study of dispersion in a heterogeneous  
 481 aquifer 4. investigation of adsorption and sampling bias. *Water Resources Re-*  
 482 *search*, *28* (12), 3325–3336.
- 483 Cho, M. S., Solano, F., Thomson, N. R., Trefry, M. G., Lester, D. R., & Metcalfe, G.  
 484 (2019). Field trials of chaotic advection to enhance reagent delivery. *Ground-*

- 485 *water Monitoring & Remediation*, 39(3), 23–39.
- 486 Cirpka, O. A. (2002). Choice of dispersion coefficients in reactive transport calculations on smoothed fields. *Journal of Contaminant Hydrology*, 58, 261282. doi: [https://doi.org/10.1016/S0169-7722\(02\)00039-6](https://doi.org/10.1016/S0169-7722(02)00039-6)
- 487
- 488
- 489 Cirpka, O. A., Frind, E. O., & Helmig, R. (1999). Numerical simulation of biodegradation controlled by transverse mixing. *Journal of Contaminant Hydrology*, 40, 159–182. doi: [https://doi.org/10.1016/S0169-7722\(99\)00044-3](https://doi.org/10.1016/S0169-7722(99)00044-3)
- 490
- 491
- 492 Cirpka, O. A., & Kitanidis, P. K. (2001). Travel-time based model of bioremediation using circulation wells. *Groundwater*, 39(3), 422–432.
- 493
- 494 Delay, F., Ackerer, P., & Danquigny, C. (2005). Simulating solute transport in porous or fractured formations using random walk particle tracking: a review. *Vadose Zone Journal*, 4(2), 360–379.
- 495
- 496
- 497 de Simoni, M., Carrera, J., Sanchez-Vila, X., & Guandagnini, A. (2005). A procedure for the solution of multicomponent reactive transport problems. *Water Resour. Res.*, 41, W11410. doi: [doi:10.1029/2005WR004056](https://doi.org/10.1029/2005WR004056)
- 498
- 499
- 500 Di Dato, M., de Barros, F. P., Fiori, A., & Bellin, A. (2018). Improving the efficiency of 3-d hydrogeological mixers: Dilution enhancement via coupled engineering-induced transient flows and spatial heterogeneity. *Water Resources Research*, 54(3), 2095–2111.
- 501
- 502
- 503
- 504 Gandhi, R. K., Hopkins, G. D., Goltz, M. N., Gorelick, S. M., & McCarty, P. L. (2002). Full-scale demonstration of in situ cometabolic biodegradation of trichloroethylene in groundwater 2. comprehensive analysis of field data using reactive transport modeling. *Water Resources Research*, 38(4), 11–1.
- 505
- 506
- 507
- 508 Gmez-Hernandez, J. J., & Wen, X.-H. (1998). To be or not to be multi-gaussian? a reflection on stochastic hydrogeology. *Advances in Water Resources*, 21, 47–61.
- 509
- 510
- 511 Harbaugh, A., Langevin, C., Hughes, J., Niswonger, R., & Konikow, L. (2017). *Modflow-2005 version 1.12.00, the us geological survey modular groundwater model: Us geological survey software release, 03 february 2017*. F7RF5S7G.
- 512
- 513
- 514 Hashemi, S., Javaherian, A., Ataee-pour, M., & Khoshdel, H. (2014). Two-point versus multiple-point geostatistics: the ability of geostatistical methods to capture complex geobodies and their facies associations an application to a channelized carbonate reservoir, southwest iran. *Journal of Geophysics and Engineering*, 11. doi: <https://doi.org/10.1088/1742-2132/11/6/065002>
- 515
- 516
- 517
- 518
- 519 Kitanidis, P. (1994). The concept of the dilution index. *Water Resour. Res.*, 30(7), 20112026.
- 520
- 521
- 522 Knudby, C., & Carrera, J. (2005). On the relationship between indicators of geostatistical, flow and transport connectivity. *Advances in Water Resources*, 28, 405–421. doi: [10.1016/j.advwatres.2004.09.001](https://doi.org/10.1016/j.advwatres.2004.09.001)
- 523
- 524
- 525 LaBolle, E. M., Quastel, J., Fogg, G. E., & Gravner, J. (2000). Diffusion processes in composite porous media and their numerical integration by random walks: Generalized stochastic differential equations with discontinuous coefficients. *Water Resources Research*, 36(3), 651–662.
- 526
- 527
- 528 Lester, D., Dentz, M., Le Borgne, T., & de Barros, F. P. J. (2018). Fluid deformation in random steady three-dimensional flow. *Journal of Fluid Mechanics*, 855, 770803. doi: [10.1017/jfm.2018.654](https://doi.org/10.1017/jfm.2018.654)
- 529
- 530
- 531 Lester, D., Metcalfe, G., Trefry, M., Ord, A., Hobbs, B., & Rudman, M. (2009). Lagrangian topology of a periodically reoriented potential flow: Symmetry, optimization, and mixing. *Physical Review E*, 80(3), 036208.
- 532
- 533
- 534 Lester, D., Rudman, M., Metcalfe, G., Trefry, M., Ord, A., & Hobbs, B. (2010). Scalar dispersion in a periodically reoriented potential flow: Acceleration via lagrangian chaos. *Physical Review E*, 81(4), 046319.
- 535
- 536
- 537 Luo, J., Wu, W.-M., Carley, J., Ruan, C., Gu, B., Jardine, P. M., . . . Kitanidis, P. K. (2007). Hydraulic performance analysis of a multiple injection–extraction well system. *Journal of Hydrology*, 336(3–4), 294–302.
- 538
- 539

- 540 MacDonald, T. R., Kitanidis, P. K., McCarty, P. L., & Roberts, P. V. (1999a).  
541 Effects of shear detachment on biomass growth and in situ bioremediation.  
542 *Groundwater*, *37*(4), 555–563.
- 543 MacDonald, T. R., Kitanidis, P. K., McCarty, P. L., & Roberts, P. V. (1999b).  
544 Mass-transfer limitations for macroscale bioremediation modeling and implica-  
545 tions on aquifer clogging. *Groundwater*, *37*(4), 523–531.
- 546 Mays, D. C., & Neupauer, R. M. (2012). Plume spreading in groundwater by  
547 stretching and folding. *Water Resources Research*, *48*(7).
- 548 McCarty, P. L., Goltz, M. N., Hopkins, G. D., Dolan, M. E., Allan, J. P., Kawakami,  
549 B. T., & Carrothers, T. (1998). Full-scale evaluation of in situ cometabolic  
550 degradation of trichloroethylene in groundwater through toluene injection.  
551 *Environmental Science & Technology*, *32*(1), 88–100.
- 552 McGregor, R., & Benevenuto, L. (2021). The effect of heterogeneity on the distribu-  
553 tion and treatment of pfas in a complex geologic environment. *Frontiers in En-  
554 vironmental Chemistry*, *2*, 729779.
- 555 Metcalfe, G., Lester, D., Trefry, M., & Ord, A. (2008). Transport in a partially open  
556 porous media flow. In *Complex systems ii* (Vol. 6802, p. 68020I).
- 557 Neupauer, R. M., Meiss, J. D., & Mays, D. C. (2014). Chaotic advection and reac-  
558 tion during engineered injection and extraction in heterogeneous porous media.  
559 *Water Resour. Res.*, *50*, 14331447. doi: doi:10.1002/2013WR014057
- 560 Piscopo, A. N., Neupauer, R. M., & Mays, D. C. (2013). Engineered injection  
561 and extraction to enhance reaction for improved in situ remediation. *Water  
562 Resour. Res.*, *49*, 3618-3625. doi: doi:10.1002/wrcr.20209
- 563 Remy, N. (2005). S-gems: the stanford geostatistical modeling software: a tool  
564 for new algorithms development. In *Geostatistics banff 2004* (pp. 865–871).  
565 Springer.
- 566 Renard, P., & Allard, D. (2013). Connectivity metrics for subsurface flow and trans-  
567 port. *Advances in Water Resources*, *51*, 168-196. doi: doi:10.1016/j.advwatres  
568 .2011.12.001
- 569 Rodriguez-Escales, P., Fernandez-Garcia, D., Drechsel, J., Folch, A., & Sanchez-  
570 Vila, X. (2017). Improving degradation of emerging organic compounds  
571 by applying chaotic advection in managed aquifer recharge in randomly  
572 heterogeneous porous media. *Water Resour. Res.*, *49*, 43764392. doi:  
573 doi:10.1002/2016WR020333
- 574 Rolle, M., Clement, T. P., Sethi, R., & Molfetta, A. D. (2008). A kinetic approach  
575 for simulating redox-controlled fringe and core biodegradation processes in  
576 groundwater: model development and application to a landfill site in piedmont,  
577 italy. *Hydrol. Process.*, *22*, 49054921. doi: 10.1002/hyp.7113
- 578 Salamon, P., Fernández-García, D., & Gómez-Hernández, J. J. (2006). A review and  
579 numerical assessment of the random walk particle tracking method. *Journal of  
580 contaminant hydrology*, *87*(3-4), 277–305.
- 581 Sather, L. J., Roth, E. J., Neupauer, R. M., Crimaldi, J. P., & Mays, D. C. (2023).  
582 Experiments and simulations on plume spreading by engineered injection and  
583 extraction in refractive index matched porous media. *Water Resources Re-  
584 search*, *59*(2), e2022WR032943.
- 585 Schulze-Makuch, D., & Cherkauer, D. (1998). Variations in hydraulic con-  
586 ductivity with scale of measurement during aquifer tests in heteroge-  
587 neous, porous carbonate rocks. *Hydrogeology Journal*, *6*, 204-215. doi:  
588 https://doi.org/10.1007/s100400050145
- 589 Sole-Mari, G., Fernandez-Garcia, D., Sanchez-Vila, X., & Bolster, D. (2019). Par-  
590 ticle density estimation with grid-projected and boundary-corrected adaptive  
591 kernels. *Advances in Water Resources*, *131*. doi: https://doi.org/10.1016/  
592 j.advwatres.2019.103382
- 593 Sole-Mari, G., Riva, M., Fernandez-Garcia, D., Sanchez-Vila, X., & Guadagnini, A.  
594 (2021). Solute transport in bounded porous media characterized by generalized

- 595 sub-gaussian log-conductivity distributions. *Advances in Water Resources*,  
596 147, 103812.
- 597 Speetjens, M., Metcalfe, G., & Rudman, M. (2021). Lagrangian transport and  
598 chaotic advection in three-dimensional laminar flows. *Applied Mechanics*  
599 *Reviews*, 73(3).
- 600 Sturman, P., Stewart, P., Cunningham, A., Bouwer, E., & Wolfram, J. (1995). Engi-  
601 neering scale-up of in situ bioremediation processes: a review. *Journal of Con-*  
602 *taminant Hydrology*, 19, 171-203. doi: [https://doi.org/10.1016/0169-7722\(95\)](https://doi.org/10.1016/0169-7722(95)00017-P)  
603 00017-P
- 604 Tartakovsky, A. M. (2010). Langevin model for reactive transport in porous media.  
605 *Physical Review E*, 82(2), 026302.
- 606 Trefry, M. G., Lester, D. R., Metcalfe, G., Ord, A., & Regenauer-Lieb, K.  
607 (2012). Toward enhanced subsurface intervention methods using chaotic  
608 advection. *Journal of Contaminant Hydrology journal*, 127, 15-29. doi:  
609 10.1016/j.jconhyd.2011.04.006
- 610 Turuban, R., Lester, D. R., Heyman, J., Borgne, T. L., & Mheust, Y. (2019).  
611 Chaotic mixing in crystalline granular media. *Journal of Fluid Mechanics*,  
612 871, 562594. doi: 10.1017/jfm.2019.245
- 613 Wang, Y., Fernández-García, D., Sole-Mari, G., & Rodríguez-Escales, P. (2022). En-  
614 hanced npl removal and mixing with engineered injection and extraction. *Wa-*  
615 *ter Resources Research*, e2021WR031114.
- 616 Zhang, P., Devries, S. L., Dathe, A., & Bagtzoglou, A. C. (2009). Enhanced mixing  
617 and plume containment in porous media under time-dependent oscillatory flow.  
618 *Environ. Sci. Technol.*, 43, 62836288. doi: 10.1021/es900854r
- 619 Zinn, B., & Harvey, C. F. (2003). When good statistical models of aquifer het-  
620 erogeneity go bad: A comparison of flow, dispersion, and mass transfer in  
621 connected and multivariate gaussian hydraulic conductivity fields. *Water*  
622 *Resources Research*, 39(3).